



FULL LENGTH ARTICLE

X-box binding protein 1 caused an imbalance in pyroptosis and mitophagy in immature rats with di-(2-ethylhexyl) phthalate-induced testis toxicity

Yifan Hong ^{a,b,c,d,e,f,g}, Xiazhu Zhou ^{a,b,c,d,e,f,g}, Qi Li ^{a,b,c,d,e,f,g},
Jing Chen ^{a,b,c,d,e,f,g}, Yuexin Wei ^{a,c,d,e,f,g},
Chunlan Long ^{b,c,d,e,f,g}, Lianju Shen ^{b,c,d,e,f,g},
Xiangqin Zheng ^{a,b,c,d,e,f,g}, Dinggang Li ^{a,b,c,d,e,f,g},
Xia Wang ^{a,b,c,d,e,f,g}, Chenjun Yu ^{a,b,c,d,e,f,g},
Shengde Wu ^{a,c,d,e,f,g,*}, Guanghui Wei ^{a,c,d,e,f,g,*}

^a Department of Urology, Children's Hospital of Chongqing Medical University, Chongqing 400014, China

^b Pediatric Research Institute, Children's Hospital of Chongqing Medical University, Chongqing 400014, China

^c Chongqing Key Laboratory of Children Urogenital Development and Tissue Engineering, Children's Hospital of Chongqing Medical University, Chongqing 400014, China

^d Chongqing Key Laboratory of Pediatrics, Children's Hospital of Chongqing Medical University, Chongqing 400014, China

^e Ministry of Education Key Laboratory of Child Development and Disorders, Children's Hospital of Chongqing Medical University, Chongqing 400014, China

^f National Clinical Research Center for Child Health and Disorders, Children's Hospital of Chongqing Medical University, Chongqing 400014, China

^g China International Science and Technology Cooperation Base of Child Development and Critical Disorders, Children's Hospital of Chongqing Medical University, Chongqing 400014, China

Received 7 November 2022; accepted 8 February 2023

Available online 27 March 2023

KEYWORDS

DEHP;

Abstract As a widely used plasticizer, di-(2-ethylhexyl) phthalate (DEHP) is known to induce significant testicular injury. However, the potential mechanism and effects of pubertal

* Corresponding author. Department of Urology, Children's Hospital of Chongqing Medical University, Chongqing 400014, China.
E-mail addresses: shengdewu@hospital.cqmu.edu.cn (S. Wu), u806806@cqmu.edu.cn (G. Wei).
Peer review under responsibility of Chongqing Medical University.

Mitophagy;
Pyroptosis;
Testicular
development;
XBP1

exposure to DEHP on testis development remain unclear. *In vivo*, postnatal day (PND) 21 male rats were gavaged with 0, 250, and 500 mg/kg DEHP for ten days. Damage to the seminiferous epithelium and disturbed spermatogenesis were observed after DEHP exposure. Meanwhile, oxidative stress-induced injury and pyroptosis were activated. Both endoplasmic reticulum (ER) stress and mitophagy were involved in this process. Monoethylhexyl phthalate (MEHP) was used as the biometabolite of DEHP *in vitro*. The GC-1 and GC-2 cell lines were exposed to 0, 100 μ M, 200 μ M, and 400 μ M MEHP for 24 h. Reactive oxygen species (ROS) generation, oxidative stress damage, ER stress, mitophagy, and pyroptosis were significantly increased after MEHP exposure. The ultrastructure of the ER and mitochondria was destroyed. X-box binding protein 1 (XBP1) was observed to be activated and translocated into the nucleus. ROS generation was inhibited by acetylcysteine. The levels of antioxidative stress, ER stress, mitophagy, and pyroptosis were decreased as well. After the administration of the ER stress inhibitor 4-phenyl-butyric acid, both mitophagy and pyroptosis were inhibited. Toyocamycin-induced XBP1 down-regulation decreased the levels of mitophagy and pyroptosis. The equilibrium between pyroptosis and mitophagy was disturbed by XBP1 accumulation. In summary, our findings confirmed that DEHP induced a ROS-mediated imbalance in pyroptosis and mitophagy in immature rat testes via XBP1. Moreover, XBP1 might be the key target in DEHP-related testis dysfunction.

© 2023 The Authors. Publishing services by Elsevier B.V. on behalf of KeAi Communications Co., Ltd. This is an open access article under the CC BY-NC-ND license (<http://creativecommons.org/licenses/by-nc-nd/4.0/>).

Introduction

Sperm quality has decreased in recent decades due to the increase in various environmental hazards.^{1,2} Approximately 50% of infertility cases worldwide result from male reproductive dysfunction.³ Among the harmful materials, the endocrine-disrupting chemical (EDC) class of chemical compounds interferes with normal spermatogenesis and causes male infertility.⁴ Once released into the environment via food packaging, polyvinyl chloride materials, toys, and baby products, EDCs enter the human body, accumulate, and exert adverse effects on diverse organ systems.⁵ Due to their estrogen-like character, EDCs disrupt both male and female gonadal development by directly causing hormone disorders or through epigenetic mechanisms, such as DNA methylation.⁶

Di-(2-ethylhexyl) phthalate (DEHP) is the most utilized plasticizer and has been shown to cause male reproductive dysfunction. DEHP is absorbed into the human body via food, water, the skin, and air.^{7,8} Increasing DEHP concentrations in urine, serum, semen, and breast milk have been recently reported.^{9–11} Additionally, urinary metabolites of DEHP are highly related to low sperm mobility and counts, reactive oxygen species (ROS) generation, and apoptosis in humans.¹² Maternal DEHP exposure may cause cryptorchidism, hypospadias, and other congenital malformations.^{13,14} Recent studies revealed decreased testosterone levels, sperm counts, and impaired testicular structure in adult rats with long-term DEHP exposure.^{15,16} Prenatal exposure to DEHP is negatively related to the adult testis volume in men.¹⁷ In addition, several studies have confirmed that DEHP exposure causes substantial harm in male animal models. In our previous study, DEHP inhibited the nuclear factor-erythroid 2 related factor (NRF2)-mediated antioxidant response and resulted in testis dysfunction by increasing the level of the m6A RNA modification in Sprague–Dawley (SD) rats.¹⁸ The integrity of the blood–testis barrier was impaired in

premature rat testes after DEHP exposure.¹⁹ Additionally, prepubertal exposure to DEHP caused apoptosis and inhibited the proliferation of both Leydig cells and Sertoli cells via the p53 signaling pathway.²⁰ Ferroptosis is also involved in somatic cell death in the testis.²¹ Pyroptosis may participate in the related injury to germ cells.²² However, the mechanism underlying DEHP-induced testicular germ cell injury has not been comprehensively clarified.

Endoplasmic reticulum (ER) stress mechanisms are activated to address the accumulation of misfolded or unfolded proteins in the ER.²³ Under ER stress conditions, cells maintain intercellular homeostasis and protein quality control systems via the unfolded protein response (UPR).²⁴ In the presence of misfolded proteins, ER stress activates the UPR and initiates the elimination of those proteins through autophagy and ER-associated degradation.²⁴ ROS may be an important activator of ER stress. Apoptosis is induced by camalexin in human leukemic cells via the ROS-ER stress-mitochondrial apoptosis pathway.²⁵ Among the three UPR branches, the endoplasmic reticulum to nucleus signaling 1 (IRE1)–X box binding protein 1 (XBP1) pathway exhibits the tightest connection with oxidative stress.^{26,27} Moreover, accumulating research has revealed a tight connection between ER stress and autophagy. Macroautophagy is activated by ROS and the UPR, depending on the context, and is crucial for irradiated cell survival.²⁷ ER stress is triggered by particulate matter <2.5 μ m (PM 2.5) and induces autophagy and apoptosis in human endothelial cells.²⁸ Ferroptosis is involved in cadmium-induced renal injury and is regulated by the MitoROS-ER stress–ferritinophagy axis.²⁹ ER stress may effectively induce autophagy. Our recent findings suggest that ROS is the factor initiating infertility after DEHP exposure.³⁰ Researchers have not clearly determined whether ER stress is involved in this process and the potential relationship between ROS and the IRE1–XBP1 pathway.

Mitophagy is a type of selective autophagy unique to the mitochondria, acting as a mitochondrial quality control mechanism that mediates the removal of impaired mitochondria.³¹ Mitophagy is also responsible for maternal mitochondrial DNA inheritance by eliminating mitochondria in the sperm.³² Damaged mitochondria are encircled by PTEN-induced putative protein kinase 1 (PINK1) and the E3 ubiquitin ligase Parkin and targeted by autophagosomes for subsequent degradation.³² PM2.5-induced vascular fibrosis is alleviated by MitoQ through a mechanism regulated by ROS/PINK1/Parkin-mediated mitophagy.³³ The NLR family pyrin domain containing 3 (NLRP3) inflammasome is activated in Parkinson's disease, and andrographolide reduces the pyroptosis level by promoting mitophagy.³⁴ A recent study also indicated that the DEHP biometabolite monoethylhexyl phthalate (MEHP) exerts cytotoxic effects via MitoROS-mediated excessive mitophagy.³⁵ In our previous study, pyroptosis was shown to be involved in DEHP-induced germ cell death.²² Thus, the role of mitophagy in DEHP-induced infertility and whether mitophagy promotes spermatogenesis by alleviating pyroptosis require further study.

In the present study, we aimed to clarify the role of ER stress in germ cell toxicity induced by DEHP and its relationship with pyroptosis to determine the role of mitophagy and the overall crucial factors involved in this process. Our findings provide new insights into DEHP-induced testicular injury in puberty and provide a novel target for preventing and treating male infertility caused by DEHP.

Materials and methods

Animals

The animal use protocol was approved by the Experimental Animal Committee of Chongqing Medical University (license number: SYXK (Yu) 2020–0001) and the Association for the Assessment and Accreditation of Laboratory Animal Care International, China. Sprague–Dawley (SD) rats were obtained from the Experimental Animal Center of Chongqing Medical University. Male offspring rats were administered corn oil (Aladdin, C116023, China) and DEHP (TCI, P0297, Japan) via gavage from postnatal days (PNDs) 21–30. All rats were sacrificed, and testes were collected on PND 31.

Animal study design

In the present study, all rats were housed in individually ventilated cages on a 12 h light/12 h dark cycle with $55\% \pm 5\%$ humidity at $25\text{ }^{\circ}\text{C} \pm 2\text{ }^{\circ}\text{C}$. The rats were given free access to water and food. PND 21 SD rats were randomly divided into three groups ($n = 10$ rats each) and administered an oral gavage of corn oil (control group) or 250/500 mg/kg body weight (bw) DEHP (the 250 mg/kg and 500 mg/kg groups) between 3:00 p.m. and 4:00 p.m. DEHP was dissolved in corn oil. Body weight was measured at the beginning and end of the study. Ulatan (20%) was used to anesthetize the rats on PND 31. Then, the rats were sacrificed by cervical dislocation. The testes were harvested and weighed. The right testes were snap-frozen in liquid nitrogen and stored at $-80\text{ }^{\circ}\text{C}$ for future protein extraction and long-term storage. The left testes were fixed with 4% paraformaldehyde (PFA)

for subsequent immunofluorescence and hematoxylin and eosin (HE) staining. The dosage of DEHP and sample sizes of the groups were based on our previous studies.^{19,22} No data points or rats were excluded. Gross morphology, western blotting, HE staining, and immunofluorescence analyses were employed to measure the main outcomes.

Histology analysis

After being fixed with 4% PFA and embedded in paraffin, testis tissues were cut into 4- μm sections. Then, the sections were deparaffinized, rehydrated, and prepared for HE staining. A light microscope (Nikon, Japan) was used to examine the sections and capture images.

Tissue immunofluorescence staining

Testis tissues were prepared and deparaffinized as described above in the section "histology analysis". Sections were immersed in a citrate solution and heated in a microwave oven for 15 min for antigen repair. Triton (0.1%, Keshi, China) and bovine serum albumin (0.5%, BSA, ZLI-9027, ZSGC-BIO) were applied for 15 min and 1 h, respectively. Primary antibodies (1:200) against NRF2 (Proteintech, 16396-1-AP) and XBP1S (Proteintech, 24868-1-AP) were used. Sections were incubated with primary antibodies at $4\text{ }^{\circ}\text{C}$ for 12 h. A fluorescein-conjugated secondary goat anti-rabbit antibody (Proteintech, SA00009-2) was applied and incubated for 1 h at room temperature in the dark. Hoechst 33342 (Beyotime, C1022) was used as a nuclear counterstain (30 min incubation at room temperature). NIS Elements Basic Research (Nikon, USA) software was used to process the images.

Cell culture and treatment

The GC-1 and GC-2 cell lines were purchased from Procell Life Science & Technology (Wuhan, China). All cell lines were used at passage numbers 5–15. The GC-1 spermatogonia cell line and GC-2 spermatocyte cell line were cultured in Dulbecco's modified Eagle's medium (DMEM, Gibco, USA) supplemented with 10% fetal bovine serum (VivaCell, Shanghai, China) and 1% penicillin and streptomycin. All cells were maintained at $37\text{ }^{\circ}\text{C}$ with 5% CO_2 in a humidified incubator. MEHP (MCE, HY-W018392, USA), acetylcysteine (synonyms: N-Acetylcysteine; N-Acetyl-L-cysteine; NAC, MCE, HY-B0215, USA), 4-phenyl-butyric acid (4-PBA, MCE, HY-A0281, USA), and toyocamycin (Toy, MCE, HY-103248, USA) were dissolved in dimethyl sulfoxide (DMSO, MCE, HY-Y0320, USA) and used in the *in vitro* study. The control group was treated with DMSO alone. NAC was added simultaneously with MEHP and maintained for 24 h. After 4-PBA or toyocamycin treatment for 4 h, MEHP was added to the cell culture medium, and the incubation continued for 24 h. The final concentration of DMSO in all groups was less than 0.1%.

Cell counting kit-8 (CCK-8) analysis

CCK-8 (NCM, C6005, China) was employed in this study to evaluate cell viability and choose the right concentration

for cell treatment. GC-1 and GC-2 cells were cultured in 96-well plates at a density of 3×10^3 cells per well. After 24 h, different concentrations of 4-PBA (0, 5, 10, 50, 100, 250, 500, 750 μM , and 1 mM) or toyocamycin (0, 0.01, 0.1, 0.5, 1, 5, 10, 20, and 40 μM) were added, and the plates were incubated for 4 h. After two washes with phosphate-buffered saline (PBS), a 10% CCK-8 solution in DMEM was added to the wells, and the plates were incubated for 2 h in the dark. A spectrophotometer was used to measure the optical density (OD) at 450 nm. No significant changes in cell viability were observed after treatment with either reagent and two relatively low concentrations (0.5 μM for 4-PBA and 0.05 μM for toyocamycin) were selected for subsequent treatments.

Isolation of nuclear/cytoplasmic proteins and mitochondrial/cytoplasmic proteins

Nuclear and cytoplasmic proteins were extracted from GC-1 and GC-2 cells using a cytoplasmic and nuclear extraction kit (Beyotime, P0027) according to the manufacturer's directions. After incubation with trypsin, cells were collected via centrifugation at 5000 rpm for 5 min. Then, they were vortexed for 5 s after the addition of cytoplasmic protein extraction reagent A and PMSF. Reagent B was added to the solution after a 10-min incubation in an ice bath. Finally, the cells were collected after centrifugation at 12,000–16,000 rcf for 5 min. The supernatant contained the target nuclear proteins. The extracted proteins were stored at -80°C until use in the Western blot analysis.

A cell mitochondria isolation kit (Beyotime, C3601) was used to extract mitochondrial and cytoplasmic proteins according to the manufacturer's instructions. The cells were collected using the process described above. After washes with PBS, the cells were collected through centrifugation at 600 rcf for 5 min. One milliliter of mitochondrial separation reagent provided in the kit was added and the cells were placed in an ice bath for 10–15 min. The cell suspension was transferred to a glass homogenizer of appropriate size and homogenized approximately 10–30 times, and the supernatant was collected after 10 min of centrifugation at 600 rcf. After a 10-min centrifugation step at 11,000 rcf, the supernatant was collected as cytoplasmic proteins, and the sediment was collected as mitochondrial proteins. The extracted proteins were used for subsequent analyses.

Western blotting

Radioimmunoprecipitation assay buffer (MCE, HY-K1001, USA) supplemented with 1% protease inhibitor cocktail (MCE, HY-K0010, USA) was utilized for protein extraction from testes and GC-1 and GC-2 cell lines. We used a bicinchoninic acid assay (Meilunbio, MA0082, China) to measure the protein concentration. After mixing with sodium dodecyl sulfate–polyacrylamide gel electrophoresis loading buffer (NCM, WB2001, China), the protein samples were boiled for 10 min. Then, the proteins were loaded onto sodium dodecyl sulfate–polyacrylamide gel electrophoresis gels, subjected to electrophoresis, and transferred to polyvinylidene fluoride (PVDF) membranes (Millipore, ISEQ00010, USA). All PVDF membranes were incubated with

blocking buffer (NCM, P30500, China) for 10 min and washed with Tris-buffered saline containing 0.1% Tween-20.

Primary antibodies (1:1000) against NRF2 (Proteintech, 16396-1-AP), superoxide dismutase (SOD, ZEN BIO, 306028), heme oxygenase 1 (HO-1, Proteintech, 10701-1-AP), ER to nucleus signaling 1 (ERN1/IRE1, Santa Cruz, sc-390960), phospho-IRE1 (Ser724) (Affinity, AF7150), eukaryotic translation initiation factor 2-a kinase 3 (EIF2AK3/PERK, Proteintech, 24390-1-AP), phospho-PERK (Thr982) (Affinity, DF7576), activating transcription factor 6 (ATF6, Proteintech, 24169-1-AP), XBP1S (Proteintech, 24868-1-AP), PTEN-induced putative kinase 1 (PINK1, ABclonal, WH219407), Parkinson disease (autosomal recessive, juvenile) 2 (PARK2/PARKIN, Proteintech, 14060-1-AP), NLRP3 (ABclonal, A5652), CASPASE1 (Abcam, ab179515), interleukin 1 beta (IL-1 β , Abcam, ab9722), interleukin 10 (IL-10, Proteintech, 20850-1-AP), LC3B (ZEN BIO, 382687), cytochrome c oxidase IV (COX IV, ZEN BIO, 200147), β -actin (ZSGB-BIO, TA-09), Lamin B1 (ZEN BIO, 380642), and β -tubulin (ZEN BIO, 380628) were used. After incubation with primary antibodies at 4°C overnight, all PVDF membranes were incubated with goat anti-rabbit IgG H&L (HRP, 1:20,000, ZEN BIO, 511203) and goat anti-mouse IgG H&L (HRP, 1:20,000, ZEN BIO, 511103), depending on the species of the primary antibody. A Super ECL Plus Kit (NCM, P10300) was used to visualize all bands. Image Lab (Bio-Rad, 3.0, USA) software was employed to quantify protein expression. The reference proteins for whole, nuclear, mitochondrial, and cytoplasmic proteins were β -actin, lamin B1, COX IV, and β -tubulin, respectively.

Total ROS and mitochondrial ROS detection

Cellular ROS generation was measured using an H_2DCFDA probe (MCE, HY-D0940). GC-1 and GC-2 cells were plated in 6-well plates at a density of 5×10^5 cells/well. After treatment with different reagents, the cells were incubated with H_2DCFDA (10 μM) for 30 min in the dark. The final fluorescence intensity was observed and images were captured using an inverted fluorescence microscope. The excitation and emission wavelengths were 488 nm and 525 nm, respectively. ImageJ (Java-based image-processing and analysis software) was used for semiquantitative analysis of the fluorescence intensity.

Mitochondrial ROS (MtSOX) were measured using MitoSOX™ red superoxide indicator (Thermo, M36008, USA). GC-1 and GC-2 cells were seeded into 6-well plates at a density of 5×10^5 cells/well. Once the treatment was complete, the cells were washed twice with PBS and incubated with MitoSOX™ red superoxide indicator (5 μM , dissolved in HBSS/Ca/Mg buffer) for 30 min in the dark. Then, the working solution was removed by washing. Hoechst 33342 was used for nuclear staining and was incubated with cells for 10 min at 37°C in the dark. An inverted fluorescence microscope was used for MtSOX detection, and ImageJ software was applied to analyze the intensity.

Scanning electron microscopy

The GC-1 and GC-2 cell lines were plated in 24-well plates. The cell count in each well was 5×10^4 cells. After

treatment, the cells were fixed with 3% glutaraldehyde overnight. Then, cell climbing sheets were washed with double-distilled water twice and dehydrated in a gradient ethanol series (30%, 50%, 70%, 80%, 90%, 95%, and 100%) for 10 min per concentration. The sheets lightly adhered to the conductive adhesive. After ion sputtering, the cells were observed using a scanning electron microscope (FEI, Inspect, USA).

Transmission electron microscopy

After DMSO or MEHP treatment, the two cell lines described above were collected and prefixed with 3% glutaraldehyde. Then, 1% osmium tetroxide was applied for postfixation. After dehydration in a series of acetone solutions, the samples were embedded in EPON 812, cut into 60–90 nm sections with a diamond knife, and stained with uranyl acetate and lead citrate. Finally, a transmission electron microscope (JEOL, JEM-1400PLUS, Japan) was used for observation.

RNA extraction and real-time quantitative PCR (RT-qPCR)

A SimplyP whole RNA extraction kit (Bioer Technology, BSC5251, China) was used to extract RNA from GC-1 and GC-2 cell lines. After extracting RNA, we used the NanoDrop ONE System (Thermo Scientific, USA) to measure the RNA concentration and the ABScript III RT Master Mix for qPCR with gDNA remover (ABclonal, RK20429, China) for reverse transcription. Complementary DNA samples were stored at -20°C for subsequent RT-qPCR. The 2X Universal SYBR Green Fast qPCR Mix (ABclonal, RK21203, China) was used for subsequent qPCR analysis. After qPCR using a CFX96 Touch Real-Time PCR Detection System (Bio-Rad, USA), we analyzed gene expression using the $2^{-\Delta\Delta\text{Ct}}$ method. β -Actin was used as the reference gene for all target genes. The primers for all genes are listed in [Supplementary Material 1](#).

Cellular immunofluorescence staining

GC-1 and GC-2 cells were plated in a 24-well plate at a density of 5×10^4 cells. After treatment, the cells were fixed with 4% PFA for 30 min and blocked with 0.5% BSA for 1 h at room temperature. Primary antibodies (1:200) against IRE1 (Santa Cruz, sc-390960), p-IRE1 (Affinity, AF7150), PINK1 (ABclonal, WH219407), XBP1S (Proteintech, 24868-1-AP), and COX IV (ZEN BIO, 200147) were applied. The cells were incubated with primary antibodies at 4°C overnight, and the subsequent procedures were performed as described in the section "tissue immunofluorescence staining".

Statistical analysis

All data in this study are presented as the mean \pm standard deviation (SD). At least 3 replicates were analyzed in each experiment. SPSS (version 22.0, Chicago, USA) was used to analyze all data. Comparisons between two groups were performed using Student's *t*-test. One-way analysis of variance (ANOVA) was used for multiple comparisons. The LSD test was used when the variance was homogeneous;

otherwise, Dunnett's T3 test was used. *P* values < 0.05 were considered statistically significant.

Results

DEHP exposure caused testicular injury in immature rats

We administered corn oil, 250 mg/kg bw DEHP, or 500 mg/kg bw DEHP to PND 21 rats by oral gavage for 10 days to determine whether DEHP would disturb spermatogenesis. The beginning and end weights of the DEHP groups were similar to those of the control group (Fig. 1B, C). No significant difference in the organ coefficient was observed between the control group and the 250 mg/kg group (Fig. 1D). However, compared with the vehicle group, the testis organ coefficient of the 500 mg/kg group was lower (Fig. 1D). Then, the histological morphology was examined. Dose-dependent DEHP-associated testicular injury was observed. Disorganization of the seminiferous epithelium, decreased germ cell numbers, and deformation of Sertoli cells was observed in the DEHP groups (Fig. 1A). Moreover, fewer layers of seminiferous epithelium were observed in both the 250 mg/kg and 500 mg/kg groups.

DEHP-induced pyroptosis in prepubertal rat testes

Oxidative stress-induced damage was observed in the DEHP-treated groups. Western blotting revealed increased levels of NRF2, the key factor in the antioxidant pathway (Fig. 1E). Levels of HO-1 and SOD, both of which are activated by NRF2, were also increased (Fig. 1E). NRF2 expression was mainly up-regulated in germ cells, based on immunofluorescence staining (Fig. 1H). The levels of key proteins involved in ER stress were measured due to their close relationship with oxidative stress. The ratios of p-PERK/PERK and p-IRE1 α /IRE1 α were also decreased (Fig. 1F). Like the factors listed above, the expression of XBP1S, the active component of XBP1, and ATF6 was down-regulated (Fig. 1F). However, in the immunofluorescence studies, although XBP1S expression in somatic cells was decreased, its expression was increased in germ cells (Fig. 1I). We measured the level of mitophagy by examining the main factors involved in this process. Both PINK1 and PARKIN expression levels were increased (Fig. 1F). Finally, NLRP3 protein levels were increased (Fig. 1G). Following activation by NLRP3, levels of the downstream proteins CASPASE1 and IL-1 β were also increased (Fig. 1G), indicating an enhanced inflammatory condition in the testis. Moreover, the expression of IL-10, an anti-inflammatory factor, was reduced. Collectively, DEHP induced oxidative stress-mediated damage in immature testes. A higher level of mitophagy was observed. Pyroptosis occurred as a result of DEHP exposure. ER stress contributes to DEHP-induced testis injury; however, its role in DEHP-related germ cell impairment remains unclear.

MEHP injured spermatogonia and spermatocytes

MEHP, the main biometabolite of DEHP, exerts a primary toxic effect on most organs.^{36,37} Based on our previous

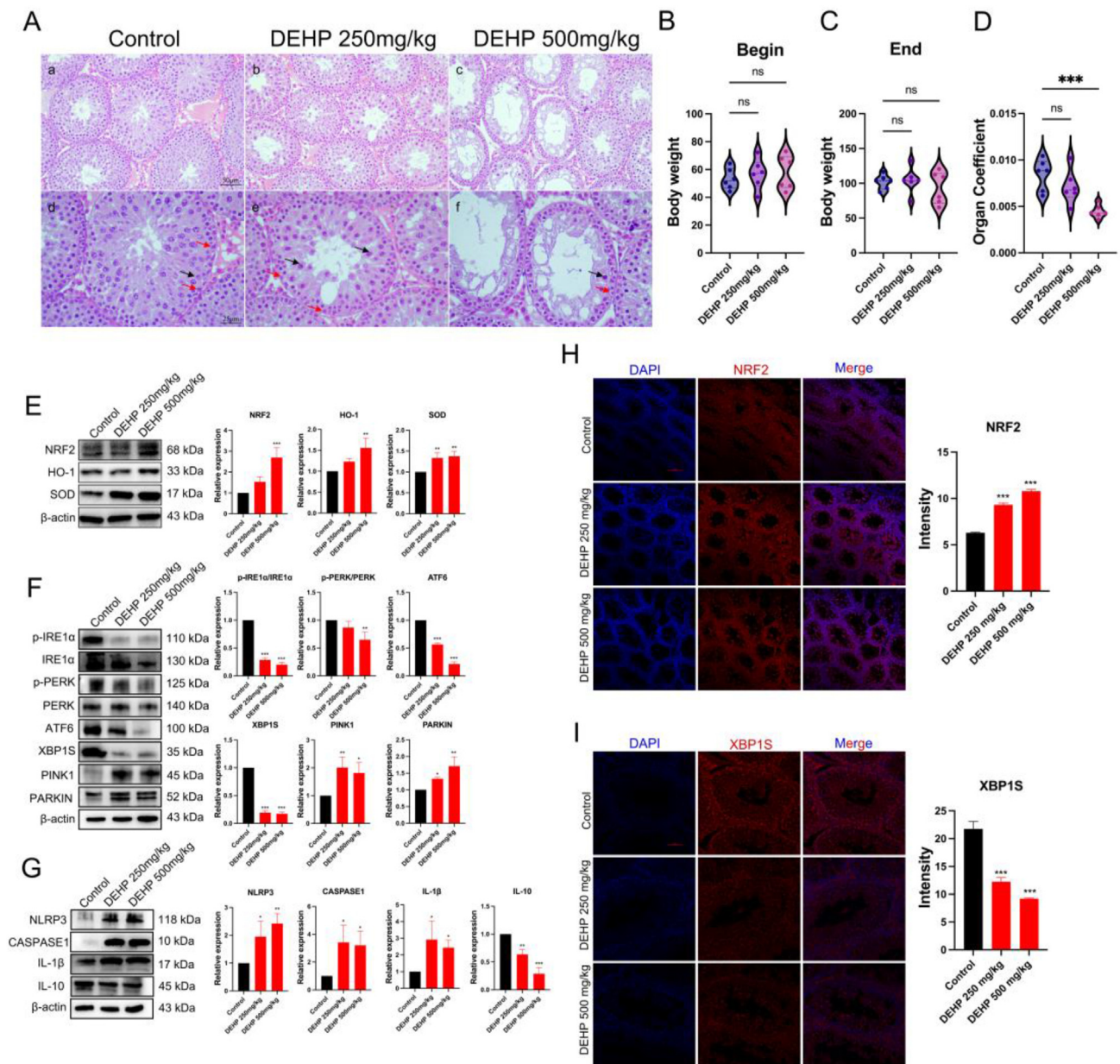


Figure 1 DEHP exposure caused testicular injury in immature rats. **(A)** Histological changes in the testes of the corn oil- and DEHP-treated groups. The vehicle group **(a, d)** showed an organized seminiferous epithelium, and spermatogenesis progressed normally. Exfoliated germ cells were observed in the 250 mg/kg group **(b, e)**. In the 500 mg/kg group **(c, f)**, atrophy of Sertoli cells and a disorganized seminiferous epithelium were noted. Black arrows indicate germ cells. Red arrows indicate Sertoli cells **(a–c)** Scale bar = 50 μ m **(d–f)** Scale bar = 25 μ m. **(B, C)** The beginning **(B)** and end **(C)** weights of the control, DEHP 250 mg/kg, and DEHP 500 mg/kg groups. No significant difference was observed among the three groups. **(D)** The testis organ coefficient of the three groups. Compared with the control group, the organ coefficient of the 500 mg/kg group was noticeably reduced. The organ coefficient of the 250 mg/kg group was similar to that of the control group. **(E)** The levels of proteins in the antioxidant pathway in immature testes. The expression levels of NRF2, HO-1 and SOD were elevated after DEHP treatment. **(F)** The ER stress and mitophagy levels of the control, 250 mg/kg, and 500 mg/kg groups. Following DEHP exposure, the expression levels of ATF6 and XBP1S were reduced, along with the p-PERK/PERK and p-IRE1 α /IRE1 α ratios. PINK1 and PARKIN expression levels were obviously increased. **(G)** The level of pyroptosis in pubertal testes. The expression levels of NLRP3, CASPASE1 and IL-1 β were significantly different in the DEHP-treated group. Compared with the control group, IL-10 expression was decreased in the other groups. This finding indicates that the anti-inflammatory response was reduced. **(H)** Immunofluorescence staining showing NRF2 expression in the three groups. Upon DEHP exposure, the intensity of NRF2 staining was increased. **(I)** Immunofluorescence staining for XBP1S in the three groups. Upon DEHP exposure, XBP1 expression in somatic cells was reduced, similar to its total intensity, while it was up-regulated in germ cells. The data were compared with the control group. One-way ANOVA was employed to analyze all the data. Each bar shows the mean \pm SD of three or more independent experiments. * P < 0.05, ** P < 0.01, *** P < 0.001.

study, MEHP was administered *in vitro*.²² Scanning electron microscopy (SEM) was used to evaluate inflammasomes in MEHP-treated cell lines (Fig. 2C). Swelling and deformation of the cells were observed in response to MEHP exposure (Fig. 2C). In the MEHP group, mitochondria-derived autophagosomes were observed (green arrows, Fig. 2D, E). The disappearance and breakage of mitochondrial cristae were also observed in the MEHP group (yellow arrows, Fig. 2D, E), indicating mitochondrial damage and mitophagy. Swollen and broken endoplasmic reticulum appeared after MEHP treatment (red arrows, Fig. 2D, E). Additionally, vacuolization was observed in MEHP-treated GC-1 cells.

Oxidative stress-induced damage and NLRP3-mediated pyroptosis were involved in MEHP-induced injury in germ cells

We measured ROS levels with the H₂DCFDA probe to confirm that ROS were generated in germ cells in response to MEHP. GC-1 spermatogonia and GC-2 spermatocytes were treated with 100 μ M, 200 μ M, or 400 μ M MEHP. In contrast to the DMSO group, ROS generation in GC-1 and GC-2 cells increased with MEHP treatment (Fig. 2A, B). MtSOX levels were also measured and were noticeably increased with MEHP treatment (Fig. 2F, G). Then, the expression levels of key factors in the antioxidant pathway were measured. NRF2

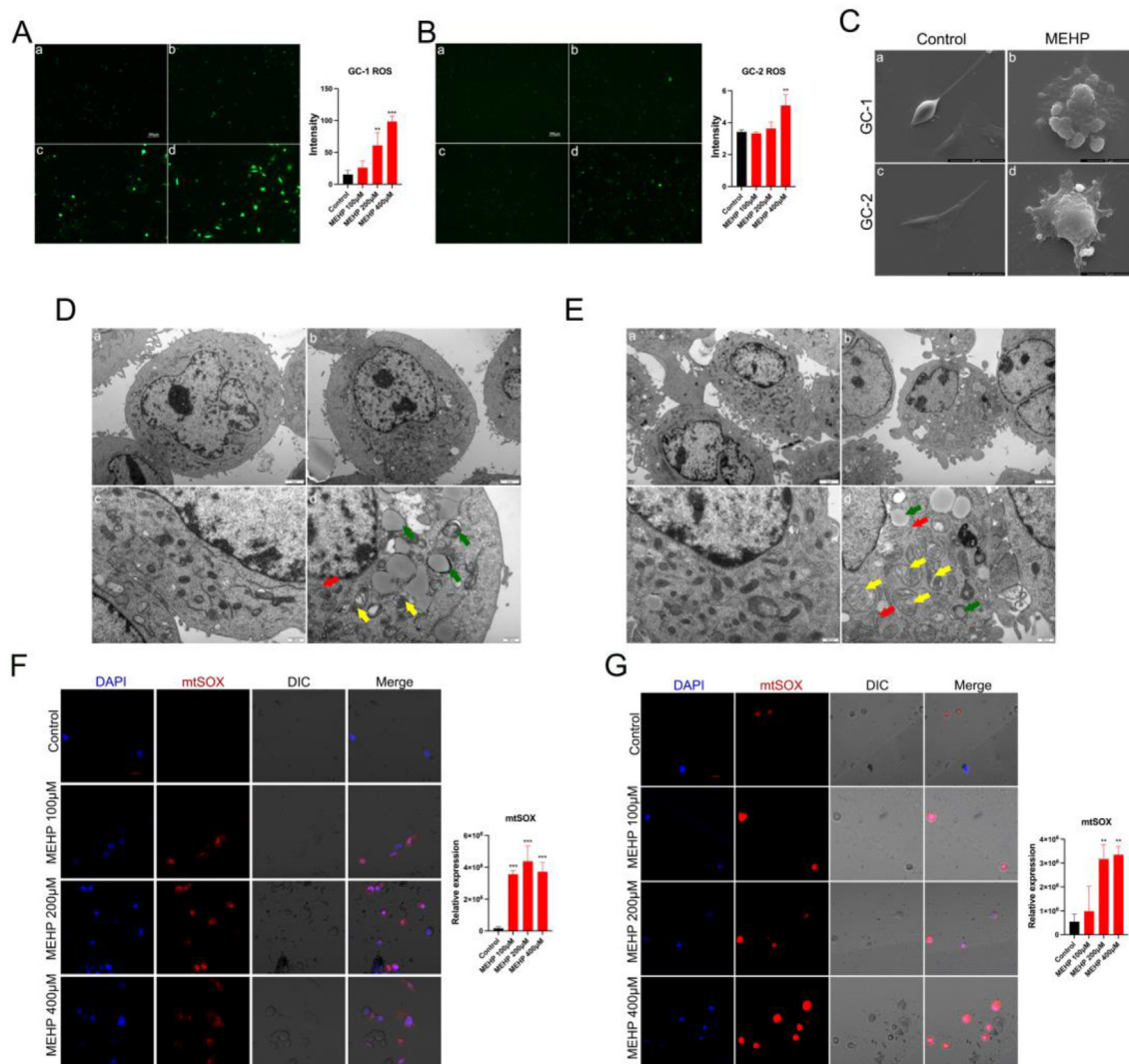


Figure 2 MEHP-induced cellular injury in GC-1 spermatogonia and GC-2 spermatocytes. (A, B) ROS generation in GC-1 and GC-2 cells. ROS generation was noticeably reduced in the MEHP groups. (C) SEM images of GC-1 (a, b) and GC-2 cells (c, d). The cells in the control groups (a, c) had a normal appearance. Inflammasomes were observed in the MEHP groups (b, d). In the MEHP groups (400 μ M), germ cells were swollen and deformed. (D, E) Transmission electron microscopy images of GC-1 (D) and GC-2 cells (E). The control group had a normal appearance (a, c). Red arrows indicate swollen or broken ER. Yellow arrows represent damaged mitochondria. The mitochondria in the MEHP group (400 μ M) (b, d) were swollen, and mitochondrial cristae were broken or missing. Green arrows represent early and mitochondria-derived autophagosomes. (F, G) Mitochondria-derived ROS generation was obviously increased in the MEHP-treated GC-1 (F) and GC-2 (G) cell lines. The data were compared with the control group. One-way ANOVA was employed to analyze all the data. Each bar shows the mean \pm SD of three or more independent experiments. ** $P < 0.01$, *** $P < 0.001$.

expression was significantly up-regulated in both MEHP-treated cell lines (Fig. 3A, B). Overall, oxidative stress and subsequent damage induced by excess ROS generation may lead to germ cell injury upon MEHP exposure.

Moreover, the levels of NLRP3 and CASPASE1, key components of the NLRP3 inflammasome, were increased (Fig. 3E, F). Consistently, IL-1 β expression was up-regulated (Fig. 3E, F), suggesting that NLRP3 was activated and initiated pyroptosis to promote the sequential maturation of pro-CASPASE1 and pro-IL-1 β . The down-regulation of IL-10 inferred the activation of downstream inflammatory pathways.

MEHP treatment increased ER stress and mitophagy

In contrast to the *in vivo* study, the expression of ATF6 and XBP1S and the ratios of p-PERK/PERK and p-IRE1 α /IRE1 α were increased in the MEHP-treated groups (Fig. 3C, D). PINK1 and PARKIN expression levels were up-regulated in the MEHP-treated group, indicating activation of the

mitophagy mechanism (Fig. 3C, D). Subsequently, immunofluorescence staining for IRE1 α , p-IRE1 α , and PINK1 was increased in germ cells (Fig. 4A–C, F). Despite the up-regulation of XBP1S expression in GC-1 and GC-2 cells, the increased translocation into the nucleus was significant (Fig. 4D). Consistent with the immunofluorescence data, the nuclear expression of XBP1S was obviously increased in the MEHP-treated group (Fig. 4J, K), suggesting that a greater effect might be exerted on the downstream pathway via the transcription factor XBP1S.

The immunofluorescence study revealed increased levels of LC3 and COX IV, mitochondrial markers, after MEHP exposure (Fig. 4E). We isolated the cytoplasm and mitochondria to confirm the mitophagy level. The mitochondrial expression of LC3 was significantly up-regulated by MEHP treatment (Fig. 4G, H).

Additionally, the mRNA expression levels of mitochondrial quality control-related genes and pathological damage-related genes were measured using RT-qPCR. *Fgf21*, a marker of mitochondrial damage, was up-regulated in both cell lines (Fig. 4I, L), indicating that MEHP induced

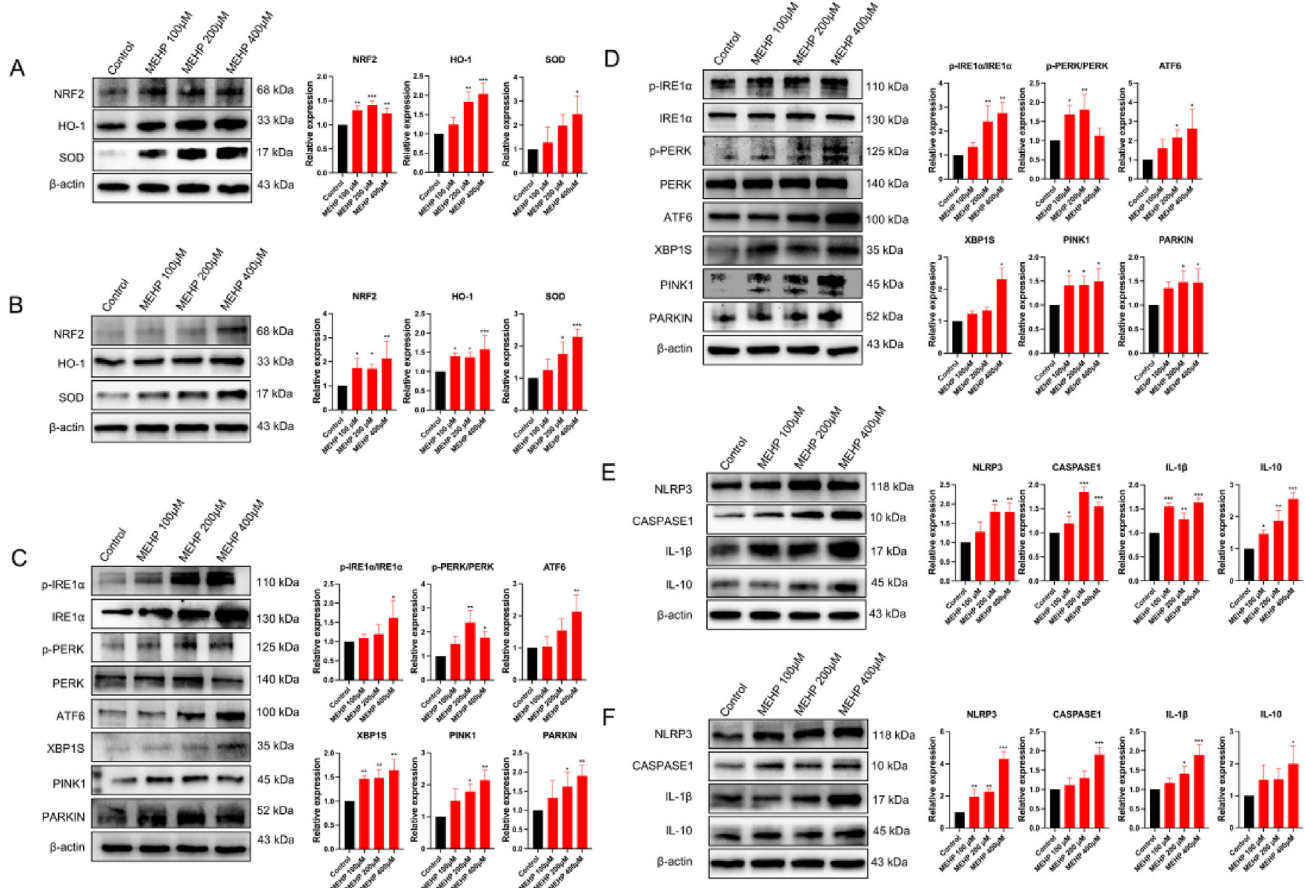


Figure 3 ER stress, mitophagy, and pyroptosis were involved in MEHP-induced germ cell damage. (A, B) The expression levels of NRF2, HO-1 and SOD were increased in GC-1 (A) and GC-2 cells (B) from the MEHP-treated groups. (C, D) The expression levels of ATF6 and XBP1S were increased, and the ratios of p-PERK/PERK and p-IRE1 α /IRE1 α in GC-1 (C) and GC-2 (D) cells were also increased, indicating an elevated ER stress level. PINK1 and PARKIN expression levels were elevated, indicating that mitophagy was activated. (E, F) Following MEHP exposure, the expression levels of NLRP3, CASPASE1, IL-1 β , and IL-10 were increased in GC-1 (E) and GC-2 cells (F). Based on these data, pyroptosis was enhanced and the levels of anti-inflammatory molecules were increased. The data were compared with the control group. One-way ANOVA was employed to analyze all the data. Each bar shows the mean \pm SD of three or more independent experiments. * P < 0.05, ** P < 0.01, *** P < 0.001.

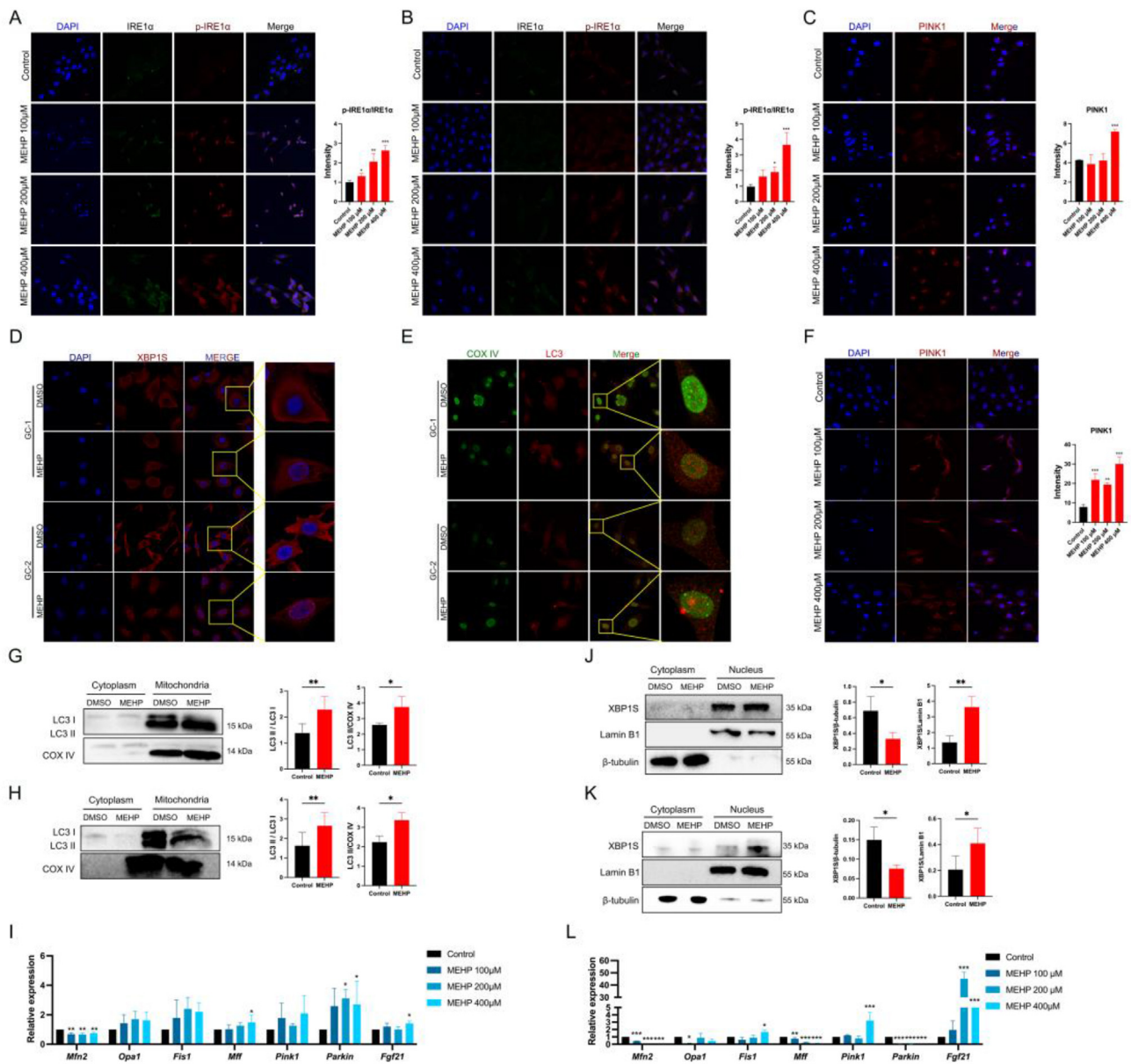


Figure 4 MEHP exposure promoted ER stress and mitophagy in germ cells. (A, B) Immunofluorescence staining for p-IRE1 α and IRE1 α in the control, 100 μ M MEHP, 200 μ M MEHP, and 400 μ M MEHP groups of GC-1 (A) and GC-2 cells (B). (C, F) PINK1 immunofluorescence staining in GC-1 (C) and GC-2 cells (F) from the four groups. (D) The expression of XBP1S in the two cell lines from the control group and MEHP group (400 μ M). With XBP1 accumulation in the MEHP group, its translocation into the nucleus was increased. (E) The co-localization of LC3 and COX IV was increased in the MEHP group of both GC-1 and GC-2 cells, indicating increased mitophagy. (G, H) Western blot analysis of LC3 and COX IV levels. In the MEHP groups of GC-1 (G) and GC-2 (H) cell lines, the levels of LC3 II/COX IV and LC3 II/LC3 I were elevated. LC3 accumulated around mitochondria. (J, K) Nuclear and cytoplasmic levels of the XBP1S, lamin B1, and β -tubulin proteins. In the MEHP groups of GC-1 (J) and GC-2 cells (K), nuclear XBP1S expression was elevated. Cytoplasmic XBP1S expression in the MEHP group was decreased. (I, L) The mRNA expression levels of key genes related to mitochondrial quality control and pathological damage in GC-1 spermatogonia (I) and GC-2 spermatocytes (L). The data were compared with the control group. One-way ANOVA was employed to analyze all the data. Each bar shows the mean \pm SD of three or more independent experiments. * P < 0.05, ** P < 0.01, *** P < 0.001.

mitochondria-related injury. Down-regulation of *Mfn2* and up-regulation of *Mff* and *Parkin* were observed in GC-1 spermatogonia (Fig. 4I). Thus, MEHP treatment inhibited mitochondrial fusion and induced mitochondrial division in GC-1 cells. A decrease in mitochondrial fusion was also observed in GC-2 spermatocytes (Fig. 4L).

ROS-initiated germ cell injury following MEHP exposure

NAC was used to confirm the factor initiating germ cell injury. ROS generation in the MEHP + NAC group was reduced in GC-1 and GC-2 cells compared with that in the

group treated with MEHP alone (Fig. 5A, E). The expression of NRF2, HO-1, and SOD was also down-regulated in the MEHP + NAC groups (Fig. 5B, C). This finding indicates that NAC inhibits ROS generation and reduces oxidative stress-induced damage in MEHP-treated germ cells.

Reduced expression of ATF6 and XBP1S was observed after NAC treatment (Fig. 5D, F). The ratios of p-PERK/PERK and p-IRE1 α /IRE1 α were also reduced (Fig. 5D, F), indicating that oxidative stress might be the main source of

ER stress in this process. Similarly, mitophagy levels were lower, and PINK1 and PARKIN expression levels were reduced (Fig. 5D, F). Pyroptosis was decreased by NAC treatment. NLRP3 and CASPASE1 are the key components of the NLRP3 inflammasome and were present at reduced levels; thus, the expression of the downstream molecule IL-1 β was down-regulated (Fig. 5H, I). In summary, excess ROS generation induced by MEHP activated the downstream pyroptosis pathway.

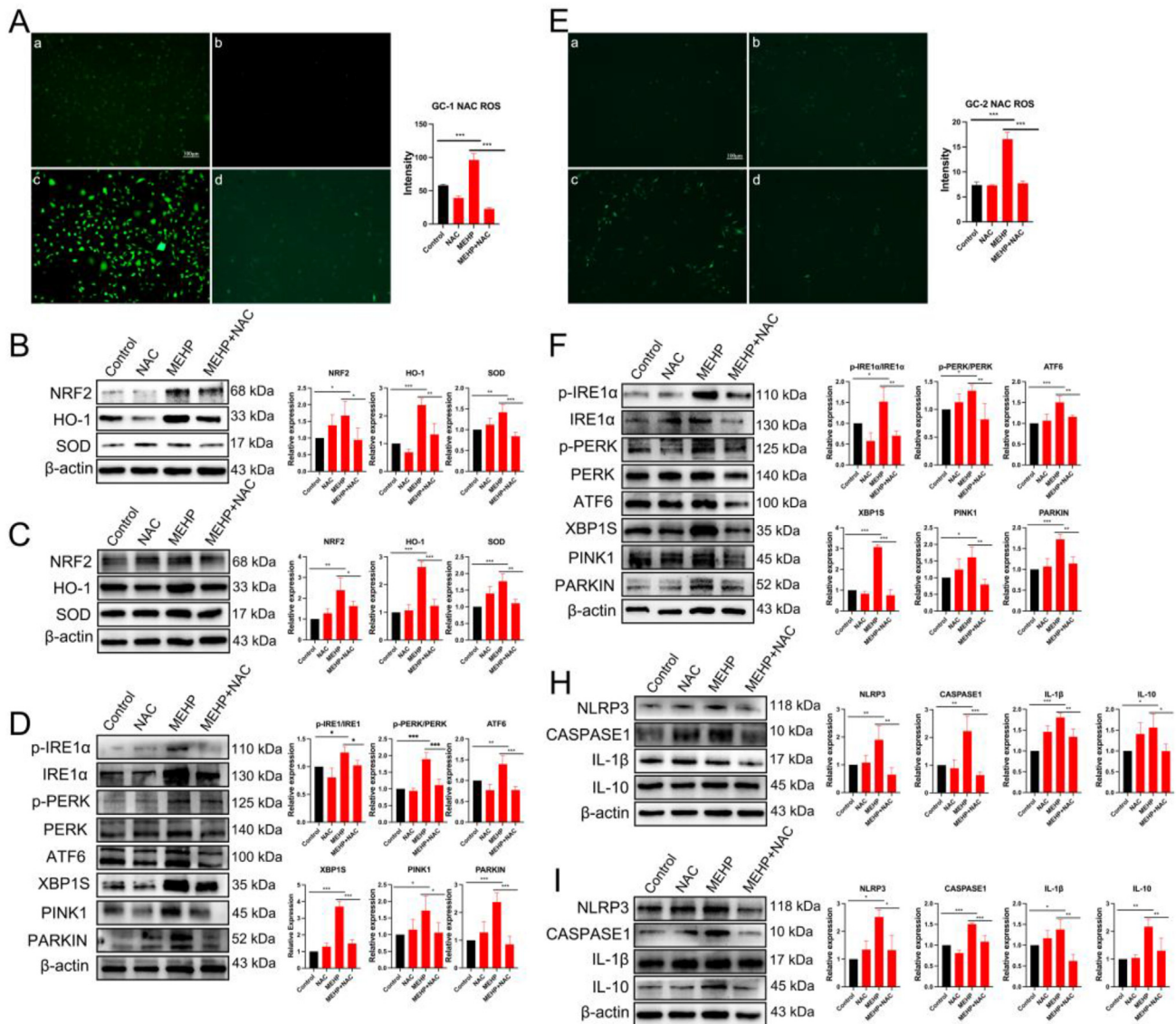


Figure 5 NAC rescued MEHP-induced germ cell injury by inhibiting ROS generation. (A, E) ROS generation in the control (a), NAC (b), MEHP (c), and MEHP + NAC (d) groups was detected. Compared with the MEHP group, ROS generation in the MEHP + NAC group was reduced by NAC in both GC-1 (A) and GC-2 (E) cells. (B, C) After the NAC intervention, the expression of NRF2, HO-1, and SOD in the MEHP + NAC group was down-regulated in GC-1 (B) and GC-2 (C) cells compared with the MEHP group. (D, F) NAC reduced the levels of ER stress-related proteins (p-PERK, PERK, p-IRE1 α , IRE1 α , ATF6, and XBP1S) and down-regulated PINK1 and PARKIN expression in both GC-1 (D) and GC-2 (F) cell lines. (H, I) After excess ROS generation was eliminated by NAC, the pyroptosis level in the MEHP + NAC group was reduced in GC-1 (H) and GC-2 (I) cells. The data were compared with the control group. One-way ANOVA was employed to analyze all the data. Each bar shows the mean \pm SD of three or more independent experiments. * P < 0.05, ** P < 0.01, *** P < 0.001.

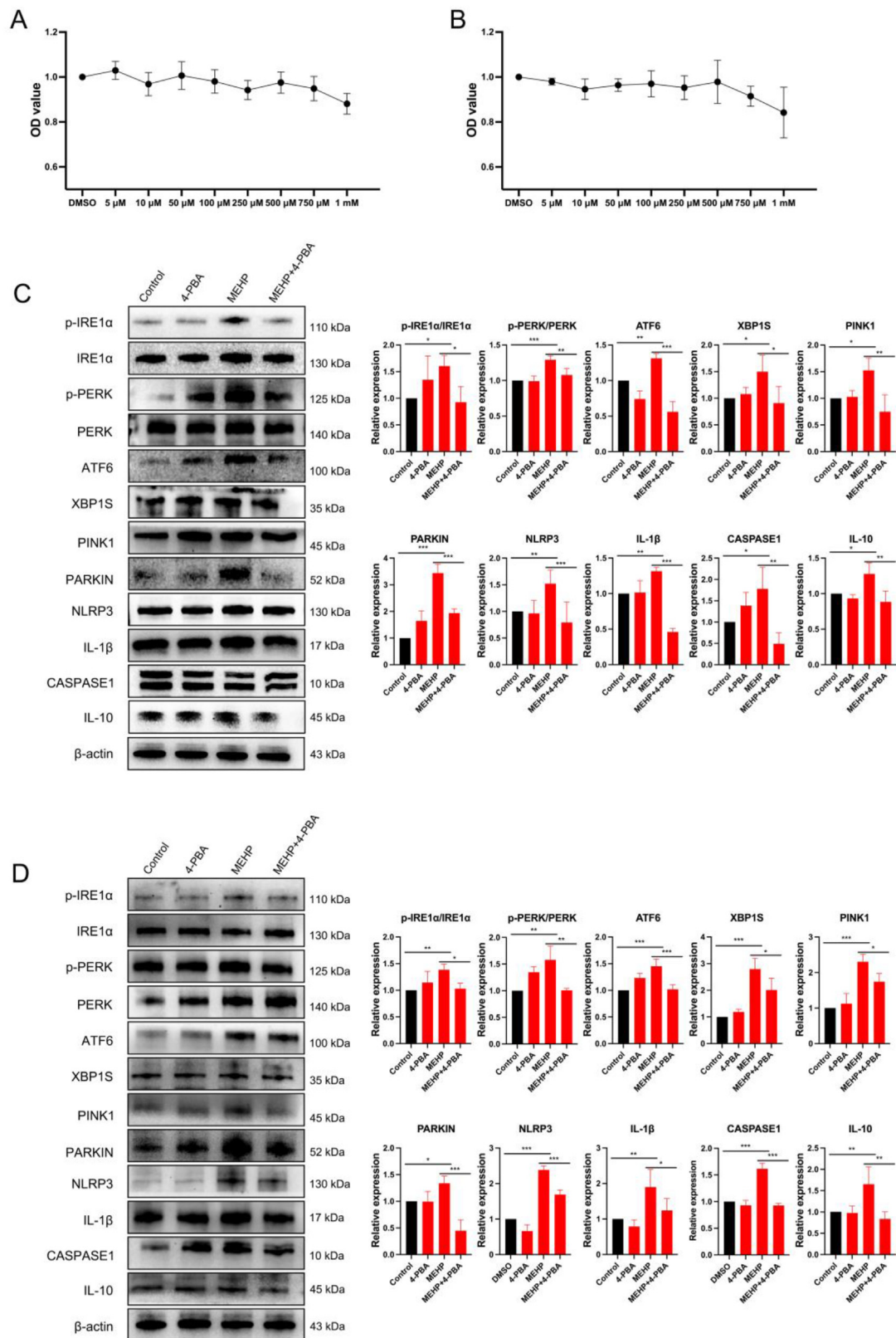


Figure 6 4-PBA inhibited ER stress and decreased MEHP-related mitophagy and pyroptosis in germ cells. **(A)** After 4-PBA treatment for 4 h, the viability and toxicity levels in GC-1 cells were measured using a CCK-8 assay. Compared with the DMSO group, no significant differences were observed after any concentration of 4-PBA. **(B)** CCK-8 data from GC-2 cells after 4 h of 4-PBA treatment. No obvious difference was observed. **(C, D)** 4-PBA inhibited ER stress in GC1 (C) and GC-2 (D) cells. The expression levels of ATF6 and XBP1S were decreased after the 4-PBA treatment. The p-PERK/PERK and p-IRE1α/IRE1α ratios were also reduced in the

4-PBA treatment reduced ER stress-induced mitophagy and pyroptosis

4-PBA was used to inhibit ER stress in the present study. Based on the results of the CCK-8 assay, we chose a relatively low and safe concentration of 4-PBA (0.5 μ M) for subsequent experiments with GC-1 and GC-2 cells (Fig. 6A, B). Reduced ratios of both p-PERK/PERK and p-IRE1 α /IRE1 α were observed (Fig. 6C, D). Similarly, the expression of key factors involved in ER stress, ATF6 and XBP1S, was down-regulated (Fig. 6C, D). When ER stress was inhibited in germ cells, decreased expression of PINK1 and PARKIN was observed in the MEHP+4-PBA group compared with the MEHP group (Fig. 6C, D). Moreover, the expression levels of NLRP3, CASPASE1, and IL-1 β were also reduced by 4-PBA, indicating a decrease in pyroptosis (Fig. 6C, D). Thus, after MEHP exposure and ROS overproduction, ER stress may trigger the pyroptosis of injured germ cells and activate mitophagy to reduce mitochondrial damage and alleviate pyroptosis.

A specific pharmacological inhibitor of XBP1 reduced MEHP-induced pyroptosis and mitophagy

Toy is a novel XBP1S-specific inhibitor. We used the CCK-8 assay to choose an appropriate concentration of Toy for GC-1 and GC-2 cell lines (Fig. 7A, B). After Toy treatment (0.05 μ M), XBP1S expression was down-regulated in GC-1 and GC-2 cells (Fig. 7C, D). The levels of p-PERK, PERK, p-IRE1 α , IRE1 α , and ATF6 were not affected by Toy (Fig. 7C, D). PINK1 and PARKIN expression levels were reduced in the MEHP + Toy group compared with the MEHP group (Fig. 7C, D). Consistent with the change in mitophagy, the expression of NLRP3, CASPASE1, and IL-1 β was also reduced by Toy (Fig. 7C, D). In conclusion, XBP1S accumulation induced mitophagy and pyroptosis.

Discussion

DEHP and its biometabolite MEHP are known for their toxicity to main organs, especially the reproductive system.^{36,38,39} Excess ROS generation, blood-testis barrier disintegration, and steroid synthesis may be triggered by DEHP exposure, as revealed in our previous studies.^{22,40} However, the potential mechanism of DEHP-induced spermatogenic dysfunction in puberty remains unclear. Protective mitophagy and pyroptosis may be activated by XBP1S accumulation and translocation. XBP1S inhibition rescued pyroptosis and reduced mitophagy. Based on these results, pubertal exposure to DEHP causes pyroptosis in germ cells by inducing ER stress, and mitophagy partially alleviates the injury. To the best of our knowledge, this study is the first to identify the key role of XBP1S in promoting mitophagy and pyroptosis (Fig. 8).

As mentioned above, puberty is the critical point of testis development and effective spermatogenesis establishment, and immature testes are more prone to injury from environmental substances.^{41,42} Due to pubertal spermatogenic disturbances, DEHP and its metabolite, MEHP, damage fertility and cause infertility in adulthood.⁴³ However, clarification of the precise mechanism of DEHP-induced testicular injury and the target factors involved in this process is an urgent need. We established an immature animal model by administering DEHP by oral gavage from PND 21 to 30 in male rats, which largely mimicked pubertal testis development. Consistent with other studies on DEHP exposure in adults, testicular injury was confirmed via histology, particularly to germ cells, and DEHP-induced male reproductive dysfunction in puberty depended on the dose.^{44,45} In our previous study, PM 2.5 led to ROS overgeneration and reproductive injury in rat testes.⁴⁶ The administration of vitamins C and E alleviated testicular damage by reducing ROS levels. Oxidative stress-induced damage was also observed in the animal and cell models used in the present study, which may indicate that ROS overgeneration and oxidative stress damage may be the main reasons for testicular damage caused by environmental toxic factors.

ER stress normally arises to manage unfolded or misfolded proteins via three downstream UPR pathways. A tight connection between ER stress and oxidative stress has been observed in recent studies.^{47–49} Additionally, excessive ER stress may induce apoptosis under extreme environmental conditions via the PERK-ATF4- DNA-damage-inducible transcript 3 (DDIT3/CHOP) pathway.⁵⁰ ER stress has also been reported to be involved in EDC-induced damage in various organs.^{28,51} However, its role and relationship with oxidative stress in DEHP-induced reproductive dysfunction, especially in immature testes, have not been explored. In the present study, ER stress was induced by MEHP-induced ROS overproduction, and NAC treatment rescued ER stress by alleviating oxidative stress and damage. NLRP3, the most important factor mediating pyroptosis, senses a variety of stimuli, such as toxins, pathogens, metabolites, crystalline substances, nucleic acids, and other environmental chemicals. Once activated by NLRP3, CASPASE1 cleaves pro-IL-1 β and pro-IL-18 to produce mature IL-1 β and IL-18, which are released through the pores formed by GSDMD, leading to pyroptosis and downstream inflammatory reactions.⁵² In the present study, the expression of NLRP3, CASPASE1, and IL-1 β in both animal and cell models was up-regulated after environmental exposure. As the gold standard of pyroptosis, the occurrence of inflammasomes in both GC-1 and GC-2 cells was observed using SEM. Moreover, consistent with other studies, the process of pyroptosis was inhibited by the NAC-induced decrease in ROS generation, suggesting that ROS are the initial factor contributing to MEHP-induced pyroptosis in germ cells.^{53,54}

MEHP+4-PBA group. PINK1 and PARKIN expression levels were down-regulated. The expression levels of core factors involved in pyroptosis, namely, NLRP3, CASPASE1, and IL-1 β , were reduced. Meanwhile, IL-10 expression was decreased, indicating a reduced anti-inflammatory level. The data were compared with the control group. One-way ANOVA was employed to analyze all the data. Each bar shows the mean \pm SD of three or more independent experiments. * P < 0.05, ** P < 0.01, *** P < 0.001.

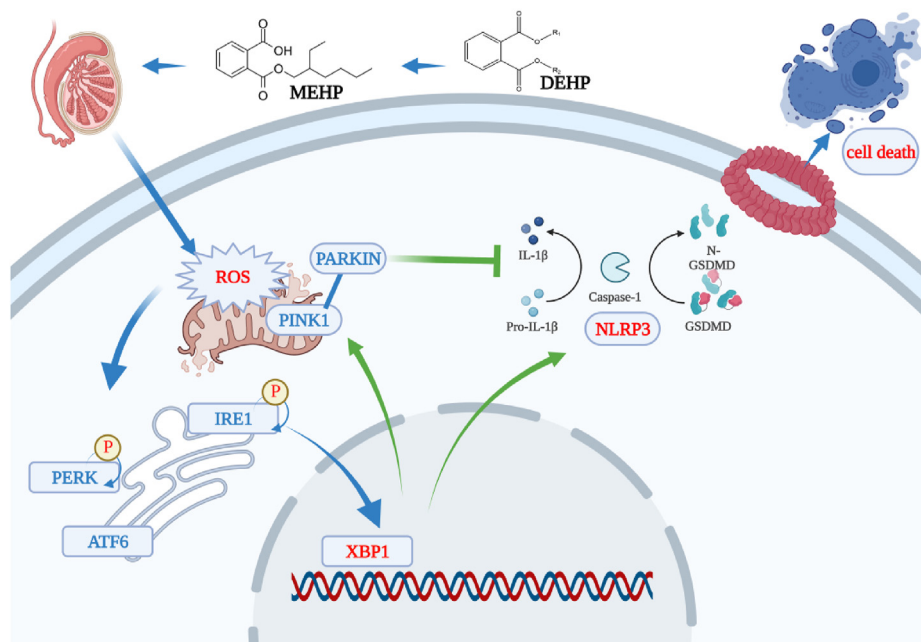


Figure 8 Schematic diagram of the proposed mechanism by which pubertal DEHP exposure induced pyroptosis in germ cells via XBP1 and the XBP1-mediated protective role of mitophagy in this process.

Mitophagy, a type of selective autophagy, functions as a double-edged sword in cellular homeostasis. Under normal circumstances, once an injury occurs, mitophagy inhibits inflammatory reactions.⁵⁵ In acute septic kidney injuries, the PINK1/PARK2/optineurin mitophagy pathway plays an important and protective role in promoting the survival of tubular cells by activating mitochondrial quality control mechanisms.⁵⁶ Upon aluminum exposure, PINK1/PARKIN-mediated mitophagy is activated and protects mouse testes from oxidative stress, apoptosis, and serious mitochondrial damage.⁵⁷ However, few studies have explored the connection between ER stress and mitophagy. The up-regulation of PINK1 and PARKIN and increased colocalization of LC3 and COX IV were observed in this study. Our findings confirmed that ER stress-induced mitophagy protected germ cells from MEHP exposure-induced death, similar to the protective role documented in other toxicity studies.^{58,59} Consistent with the findings of our previous study, pyroptosis was also observed in these cells. Moreover, 4-PBA rescued MEHP-injured germ cells undergoing pyroptosis. This finding indicated that pyroptosis was also induced by ER stress.

As the testes comprise a mix of germ cells, Sertoli cells, Leydig cells, and other somatic cells, testis protein expression levels may not indicate the true condition of spermatogonia and spermatocytes. Moreover, increased XBP1S expression in germ cells was observed using immunofluorescence staining. XBP1S is the main effector of the IRE1–XBP1 pathway involved in ER stress. Under oxidative stress conditions, XBP1S protects the kidney from ischemia–reperfusion injury by activating mitophagy.⁶⁰ XBP1S activated by ROS may also participate in the patulin-induced apoptosis of human intestinal and kidney cells.⁶¹ Several studies have explored the role of ER stress in testicular injury under different conditions, such

as aging and human chorionic gonadotropin exposure.^{62,63} ER stress was shown to trigger apoptosis in the aforementioned testis damage models. However, little is known about its role in environmental toxicity-related male reproductive dysfunction, especially that caused by DEHP, and more importantly, whether the downstream effector XBP1 plays an important role in this process. We utilized Toy as a novel XBP1-specific inhibitor in this study to elucidate the currently unclear role of XBP1S. After Toy administration, PINK1 and PARKIN expression levels were reduced and decreased expression of NLRP3, CASPASE1, and IL-1 β was also observed. Thus, both mitophagy and pyroptosis were induced by XBP1. XBP1 is the key factor contributing to MEHP-induced germ cell death. Further research should focus on the role of this activator.

This study has some limitations. First, although Toy specifically inhibits XBP1 as a novel inhibitor, researchers have not clearly determined whether Toy affects the activity of other factors in the pathway. Thus, the knockdown of XBP1 in germ cells and the *Xbp1* knockout rat model will be more suitable models for analysis. Furthermore, chromatin immunoprecipitation (ChIP) and ChIP–qPCR experiments are needed to confirm the effectiveness of XBP1 as a transcription factor. Additionally, while mitophagy exerts a protective effect under normal conditions, excess mitophagy causes cell death under some extreme conditions. For instance, oxygen-glucose deprivation/reoxygenation-induced neuronal injury is aggravated by the lncRNA SNHG14 via excess mitophagy induced by the miR-182–5p/BINP3 axis.⁶⁴ Thus, studies investigating the activation and inhibition of mitophagy may be necessary. Moreover, the high dose of DEHP applied to immature rats may not be equivalent to the daily dose to which humans are exposed, and the potential mechanism of low-dose, longer-term DEHP exposure in mammals may be different from that

identified in this study. Subsequent studies focused on low-dose DEHP exposure and *Xbp1* knockout rat models should be considered.

In conclusion, the present study reveals that ROS-mediated pyroptosis is involved in the DEHP-induced spermatogenesis disturbance in puberty. The key effector of ER stress, XBP1, is activated by excess ROS generation and increases pyroptosis following the up-regulation of IRE1 α . XBP1-induced mitophagy may have a protective function in this process. Our findings confirm that XBP1 is involved in DEHP-induced injury in immature testes and provide new ideas for further toxicology research on infertility resulting from DEHP exposure in puberty.

Author contributions

Yifan Hong, Chunlan Long, and Shengde Wu: conceptualization, methodology, and writing – original draft preparation; Yifan Hong, Xiazhu Zhou, Shengde Wu, and Qi Li: data curation and software; Yifan Hong, Jing Chen, Xiangqin Zheng, and Xia Wang: visualization and investigation; Lianju Shen, Chunlan Long, and Guanghui Wei: supervision; Yuexin Wei, Yifan Hong, Dinggang Li, and Chenjun Yu: software and validation; Guanghui Wei, Chunlan Long, Shengde Wu, and Yifan Hong: writing – review & editing.

Conflict of interests

The authors declare that they have no known competing financial interests or personal relationships that could have appeared to influence the work reported in this paper.

Funding

This study was supported by the National Natural Science Foundation of China (No. 81771566, 82071632), the Postgraduate Research Innovation Project of Chongqing Medical University (China) (No. CYB22210), and the Youth Basic Research Project from the Ministry of Education Key Laboratory of Child Development and Disorders (China) (No. YBRP-202114).

Acknowledgements

Our graphical abstract and schematic diagrams were created using the BioRender website (app. [biorender.com](https://www.biorender.com)). We thank AJE (www.aje.cn) for the language editing services.

Appendix A. Supplementary data

Supplementary data to this article can be found online at <https://doi.org/10.1016/j.gendis.2023.02.030>.

References

1. Yang Y, Zhang H, Wang S, et al. Variation in sperm morphology and performance in tree sparrow (*Passer montanus*) under long-term environmental heavy metal pollution. *Ecotoxicol Environ Saf.* 2020;197:110622.
2. Zhao Y, Zhu Q, Lin J, et al. Association of exposure to particulate matter air pollution with semen quality among men in China. *JAMA Netw Open.* 2022;5(2):e2148684.
3. Kilchevsky A, Honig S. Male factor infertility in 2011: semen quality, sperm selection and hematospermia. *Nat Rev Urol.* 2012;9(2):68–70.
4. Oluwayiose OA, Marcho C, Wu H, et al. Paternal preconception phthalate exposure alters sperm methylome and embryonic programming. *Environ Int.* 2021;155:106693.
5. Yilmaz B, Terekeci H, Sandal S, et al. Endocrine disrupting chemicals: exposure, effects on human health, mechanism of action, models for testing and strategies for prevention. *Rev Endocr Metab Disord.* 2020;21(1):127–147.
6. Sifakis S, Androutsopoulos VP, Tsatsakis AM, et al. Human exposure to endocrine disrupting chemicals: effects on the male and female reproductive systems. *Environ Toxicol Pharmacol.* 2017;51:56–70.
7. Di Nisio A, Foresta C. Water and soil pollution as determinant of water and food quality/contamination and its impact on male fertility. *Reprod Biol Endocrinol.* 2019;17:4.
8. Di Nisio A, Sabovic I, Valente U, et al. Endocrine disruption of androgenic activity by perfluoroalkyl substances: clinical and experimental evidence. *J Clin Endocrinol Metab.* 2019;104(4):1259–1271.
9. Saab Y, Oueis E, Mehanna S, et al. Risk assessment of phthalates and their metabolites in hospitalized patients: a focus on di- and mono-(2-ethylhexyl) phthalates exposure from intravenous plastic bags. *Toxics.* 2022;10(7):357.
10. Henriksen LS, Mathiesen BK, Assens M, et al. Use of stored serum in the study of time trends and geographical differences in exposure of pregnant women to phthalates. *Environ Res.* 2020;184:109231.
11. Long SE, Kahn LG, Trasande L, et al. Urinary phthalate metabolites and alternatives and serum sex steroid hormones among pre- and postmenopausal women from NHANES, 2013–16. *Sci Total Environ.* 2021;769:144560.
12. Huang LP, Lee CC, Fan JP, et al. Urinary metabolites of di-(2-ethylhexyl) phthalate relation to sperm motility, reactive oxygen species generation, and apoptosis in polyvinyl chloride workers. *Int Arch Occup Environ Health.* 2014;87(6):635–646.
13. Zhou Y, Huang F, Liu Y, et al. TGF- β 1 relieves epithelial-mesenchymal transition reduction in hypospadias induced by DEHP in rats. *Pediatr Res.* 2020;87(4):639–646.
14. Skinner MK. Endocrine disruptors in 2015: epigenetic trans-generational inheritance. *Nat Rev Endocrinol.* 2016;12(2):68–70.
15. Oudir M, Chader H, Bouzid B, et al. Male rat exposure to low dose of di-(2-ethylhexyl) phthalate during pre-pubertal, pubertal and post-pubertal periods: impact on sperm count, gonad histology and testosterone secretion. *Reprod Toxicol.* 2018;75:33–39.
16. Chang WH, Herianto S, Lee CC, et al. The effects of phthalate ester exposure on human health: a review. *Sci Total Environ.* 2021;786:147371.
17. Hart RJ, Frederiksen H, Doherty DA, et al. The possible impact of antenatal exposure to ubiquitous phthalates upon male reproductive function at 20 years of age. *Front Endocrinol.* 2018;9:288.
18. Zhao TX, Wang JK, Shen LJ, et al. Increased m6A RNA modification is related to the inhibition of the Nrf 2-mediated antioxidant response in di-(2-ethylhexyl) phthalate-induced prepubertal testicular injury. *Environ Pollut.* 2020;259:113911.
19. Wei Y, Tang XL, Zhou Y, et al. DEHP exposure destroys blood-testis barrier (BTB) integrity of immature testes through

- excessive ROS-mediated autophagy. *Genes Dis.* 2018;5(3): 263–274.
20. Wang J, Zhao T, Chen J, et al. Multiple transcriptomic profiling: p53 signaling pathway is involved in DEHP-induced prepubertal testicular injury via promoting cell apoptosis and inhibiting cell proliferation of Leydig cells. *J Hazard Mater.* 2021;406:124316.
 21. Wu Y, Wang J, Zhao T, et al. Di-(2-ethylhexyl) phthalate exposure leads to ferroptosis via the HIF-1 α /HO-1 signaling pathway in mouse testes. *J Hazard Mater.* 2022;426:127807.
 22. Hong Y, Zhou Y, Shen L, et al. Exposure to DEHP induces testis toxicity and injury through the ROS/mTOR/NLRP3 signaling pathway in immature rats. *Ecotoxicol Environ Saf.* 2021;227: 112889.
 23. Rashid HO, Yadav RK, Kim HR, et al. ER stress: autophagy induction, inhibition and selection. *Autophagy.* 2015;11(11): 1956–1977.
 24. Hetz C, Zhang K, Kaufman RJ. Mechanisms, regulation and functions of the unfolded protein response. *Nat Rev Mol Cell Biol.* 2020;21(8):421–438.
 25. Yang Y, Wang G, Wu W, et al. Camalexin induces apoptosis via the ROS-ER stress-mitochondrial apoptosis pathway in AML cells. *Oxid Med Cell Longev.* 2018;2018:7426950.
 26. Zou J, Fei Q, Xiao H, et al. VEGF-A promotes angiogenesis after acute myocardial infarction through increasing ROS production and enhancing ER stress-mediated autophagy. *J Cell Physiol.* 2019;234(10):17690–17703.
 27. Chaurasia M, Gupta S, Das A, et al. Radiation induces EIF2AK3/PERK and ERN1/IRE1 mediated pro-survival autophagy. *Autophagy.* 2019;15(8):1391–1406.
 28. Wang Y, Tang M. PM_{2.5} induces autophagy and apoptosis through endoplasmic reticulum stress in human endothelial cells. *Sci Total Environ.* 2020;710:136397.
 29. Zhao C, Yu D, He Z, et al. Endoplasmic reticulum stress-mediated autophagy activation is involved in cadmium-induced ferroptosis of renal tubular epithelial cells. *Free Radic Biol Med.* 2021;175:236–248.
 30. Zhao TX, Wei YX, Wang JK, et al. The gut-microbiota-testis axis mediated by the activation of the Nrf 2 antioxidant pathway is related to prepubertal steroidogenesis disorders induced by di-(2-ethylhexyl) phthalate. *Environ Sci Pollut Res.* 2020;27(28): 35261–35271.
 31. Pickles S, Vigié P, Youle RJ. Mitophagy and quality control mechanisms in mitochondrial maintenance. *Curr Biol.* 2018; 28(4):R170–R185.
 32. Ashrafi G, Schwarz TL. The pathways of mitophagy for quality control and clearance of mitochondria. *Cell Death Differ.* 2013;20(1):31–42.
 33. Ning R, Li Y, Du Z, et al. The mitochondria-targeted antioxidant MitoQ attenuated PM_{2.5}-induced vascular fibrosis via regulating mitophagy. *Redox Biol.* 2021;46:102113.
 34. Ahmed S, Kwatra M, Ranjan Panda S, et al. Andrographolide suppresses NLRP3 inflammasome activation in microglia through induction of parkin-mediated mitophagy in *in-vitro* and *in-vivo* models of Parkinson disease. *Brain Behav Immun.* 2021;91:142–158.
 35. Xu J, Wang L, Zhang L, et al. Mono-2-ethylhexyl phthalate drives progression of PINK1-parkin-mediated mitophagy via increasing mitochondrial ROS to exacerbate cytotoxicity. *Redox Biol.* 2021;38:101776.
 36. Li A, Kang L, Li R, et al. Modeling di (2-ethylhexyl) phthalate (DEHP) and its metabolism in a body's organs and tissues through different intake pathways into human body. *Int J Environ Res Publ Health.* 2022;19(9):5742.
 37. Zhao Y, Song X, Ding S, et al. The associations of urinary DEHP metabolite levels, serum thyroid hormones, and thyroid-related genes among the adolescent students from China: a cross-sectional study. *Environ Sci Pollut Res.* 2022;29(13): 19081–19097.
 38. Takdastan A, Niari MH, Babaei A, et al. Occurrence and distribution of microplastic particles and the concentration of Di 2-ethyl hexyl phthalate (DEHP) in microplastics and wastewater in the wastewater treatment plant. *J Environ Manag.* 2021;280:111851.
 39. Zheng S, Wang J, Zhuo Y, et al. Spatial distribution model of DEHP contamination categories in soil based on Bi-LSTM and sparse sampling. *Ecotoxicol Environ Saf.* 2022;229: 113092.
 40. Han L, Wang J, Zhao T, et al. Stereological analysis and transcriptome profiling of testicular injury induced by di-(2-ethylhexyl) phthalate in prepubertal rats. *Ecotoxicol Environ Saf.* 2021;220:112326.
 41. Edwards TM, Hamlin HJ. Reproductive endocrinology of environmental nitrate. *Gen Comp Endocrinol.* 2018;265:31–40.
 42. Terayama H, Qu N, Endo H, et al. Effect of acetamiprid on the immature murine testes. *Int J Environ Health Res.* 2018;28(6): 683–696.
 43. Liu L, Wang H, Tian M, et al. Phthalate metabolites related to infertile biomarkers and infertility in Chinese men. *Environ Pollut.* 2017;231:291–300.
 44. Fiandane N, Borromeo V, Berrini A, et al. Maternal exposure to a mixture of di(2-ethylhexyl) phthalate (DEHP) and polychlorinated biphenyls (PCBs) causes reproductive dysfunction in adult male mouse offspring. *Reprod Toxicol.* 2016;65: 123–132.
 45. Andrade AJM, Grande SW, Talsness CE, et al. A dose response study following *in utero* and lactational exposure to di-(2-ethylhexyl) phthalate (DEHP): reproductive effects on adult male offspring rats. *Toxicology.* 2006;228(1):85–97.
 46. Liu B, Wu SD, Shen LJ, et al. Spermatogenesis dysfunction induced by PM_{2.5} from automobile exhaust via the ROS-mediated MAPK signaling pathway. *Ecotoxicol Environ Saf.* 2019; 167:161–168.
 47. Lin Y, Jiang M, Chen W, et al. Cancer and ER stress: mutual crosstalk between autophagy, oxidative stress and inflammatory response. *Biomed Pharmacother.* 2019;118:109249.
 48. Zhao T, Wu K, Hogstrand C, et al. Lipophagy mediated carbohydrate-induced changes of lipid metabolism via oxidative stress, endoplasmic reticulum (ER) stress and ChREBP/PPAR γ pathways. *Cell Mol Life Sci.* 2020;77(10):1987–2003.
 49. Yin Y, Sun G, Li E, et al. ER stress and impaired autophagy flux in neuronal degeneration and brain injury. *Ageing Res Rev.* 2017;34:3–14.
 50. Yi S, Chen K, Zhang L, et al. Endoplasmic reticulum stress is involved in stress-induced hypothalamic neuronal injury in rats via the PERK-ATF4-CHOP and IRE1-ASK1-JNK pathways. *Front Cell Neurosci.* 2019;13:190.
 51. Takanezawa Y, Nakamura R, Sugimoto T, et al. p62/sequestrin 1 attenuates methylmercury-induced endoplasmic reticulum stress in mouse embryonic fibroblasts. *Toxicol Lett.* 2021;353:93–99.
 52. Yu P, Zhang X, Liu N, et al. Pyroptosis: mechanisms and diseases. *Signal Transduct Targeted Ther.* 2021;6:128.
 53. Zhou B, Zhang JY, Liu XS, et al. Tom 20 senses iron-activated ROS signaling to promote melanoma cell pyroptosis. *Cell Res.* 2018;28(12):1171–1185.
 54. Wu X, Zhang H, Qi W, et al. Nicotine promotes atherosclerosis via ROS-NLRP3-mediated endothelial cell pyroptosis. *Cell Death Dis.* 2018;9(2):171.
 55. Lin Q, Li S, Jiang N, et al. Inhibiting NLRP3 inflammasome attenuates apoptosis in contrast-induced acute kidney injury

- through the upregulation of HIF1A and BNIP₃-mediated mitophagy. *Autophagy*. 2021;17(10):2975–2990.
56. Wang Y, Zhu J, Liu Z, et al. The PINK1/PARK2/optineurin pathway of mitophagy is activated for protection in septic acute kidney injury. *Redox Biol*. 2021;38:101767.
 57. Liu M, Wang B, Cui Y, et al. PINK1/Parkin-mediated mitophagy is activated to protect against testicular damage caused by aluminum. *J Inorg Biochem*. 2022;232:111840.
 58. Liu P, Guo C, Cui Y, et al. Activation of PINK1/Parkin-mediated mitophagy protects against apoptosis in kidney damage caused by aluminum. *J Inorg Biochem*. 2022;230:111765.
 59. Guo C, Liu Y, Wang Y, et al. PINK1/Parkin-mediated mitophagy is activated to protect against AFB₁-induced immunosuppression in mice spleen. *Toxicol Lett*. 2022;366:33–44.
 60. Liu Z, Wang M, Wang X, et al. XBP1 deficiency promotes hepatocyte pyroptosis by impairing mitophagy to activate mtDNA-cGAS-STING signaling in macrophages during acute liver injury. *Redox Biol*. 2022;52:102305.
 61. Boussabbeh M, Ben Salem I, Prota A, et al. Patulin induces apoptosis through ROS-mediated endoplasmic reticulum stress pathway. *Toxicol Sci*. 2015;144(2):328–337.
 62. Park SJ, Kim TS, Park CK, et al. hCG-induced endoplasmic reticulum stress triggers apoptosis and reduces steroidogenic enzyme expression through activating transcription factor 6 in Leydig cells of the testis. *J Mol Endocrinol*. 2013;50(2):151–166.
 63. Zhao H, Ma N, Chen Q, et al. Decline in testicular function in ageing rats: changes in the unfolded protein response and mitochondrial apoptotic pathway. *Exp Gerontol*. 2019;127:110721.
 64. Deng Z, Ou H, Ren F, et al. LncRNA SNHG14 promotes OGD/R-induced neuron injury by inducing excessive mitophagy via miR-182-5p/BNIP₃ axis in HT22 mouse hippocampal neuronal cells. *Biol Res*. 2020;53(1):38.